Numerical investigation on laminar round-jet impinging on a surface at uniform heat flux in a channel partially filled with a porous medium

B Buonomo[1], A Diana[2], O Manca[1,*], S Nardini[1]

[1]Dipartimento di Ingegneria Industriale e dell'Informazione, Seconda Università degli Studi di Napoli, Via Roma 29, 81031 Aversa, Italy
[2]Dipartimento di Ingegneria Meccanica, Energetica, Gestionale e dei Trasporti, Università degli Studi di Genova, Genova (GE), Italy

*Corresponding author: oronzio.manca@unina2.it

Abstract. Horizontal channel partially filled with porous media and a single round jet impinging on the porous medium are numerically investigated. The wall facing the round jet is partially heated at uniform heat flux. A two-dimensional axial symmetric flow in the channel is assumed to evaluate the thermal behavior within the channel. The analysis in the porous medium is accomplished in local thermal equilibrium conditions and under the Brinkman–Forchheimer-extended Darcy law assumption. The problem is solved employing the Ansys-Fluent code. Results are given in terms of stream function and temperature fields of fluid and solid matrix, wall temperature profiles, air velocity and temperature profiles along the transversal section of channel. The Peclet number ranges from 1 to 1000 and Rayleigh number values are 10, 50, 100 and 1000. Reynolds jet number, solid wall distance and wall heat flux effects on thermal and fluid dynamic behaviors are investigated. Results indicate that Nusselt number has the highest value for the channel with a porous medium of thickness equal to the channel gap, whereas it presents very small changes increasing the porous medium length on the heated wall. Correlations among average Nusselt, Peclet and Rayleigh numbers are proposed.

1. Introduction

Heat transfer enhancement technologies play an important role in several applications, in terms of technical advantages and cost savings. Jet impingement of a cold fluid is an efficient cooling method of a heated surface, especially if jets are employed with porous media, like aluminum foams. As indicated in literature, jets are becoming important in many engineering applications, as turbine blade internal cooling, electronic cooling systems, solar collectors, food and drying technologies, combustion and anti-icing systems, etc [1-6]. Several parameters, like porosity and thermal conductivity, have effects on the fluid and thermal behaviors and they are investigated to evaluate optimal configurations in order to enhance the heat transfer. First studies on laminar impinging jets on a porous medium are carried out numerically and experimentally, considering the channel totally or partially filled in [7-12]. In [13-16], an impinging slot jet is numerically studied considering mixed convection, Darcy and local thermal equilibrium (LTE) and local thermal non-equilibrium (LTNE) models. In [17-21], the effect of opposite mixed convection on the jet impingement cooling of a partially heated surface is investigated at assigned temperature in a confined porous channel. In [22], impinging laminar jet on an array of discrete protruding heat sources without and with a porous layer is studied thanks to generalized Darcy–Forchheimer–Brinkman and LTE models. In [23, 24] experimental studies of a round, impinging-jet flowing through metallic foam with restricted flow outlets are performed, considering different values of porosity, pore density, length of sample, air velocity and flow outlet height. In [25, 26] a confined, round, laminar impinging jet, fed upward against the gravity, is numerically and experimentally studied, under the influence of an impingement-surface heating.

In this work, a parallel-plate channel partially filled with a high permeability porous medium with a single round jet impinging on the porous medium is numerically investigated. The opposite wall to the air round jet is partially heated at uniform heat flux. The fluid flow in the channel is assumed as two dimensional and the porous medium is modeled using the Brinkman–Forchheimer-extended Darcy model, taking account of viscosity and inertia effects. The structure of the porous medium is homogenous and isotropic, the thermophysical properties of the air and the porous medium are considered temperature independent and the fluid flow is steady state, laminar and incompressible. The analysis in the porous medium is accomplished under LTE conditions and a two-dimensional numerical axial symmetric model is developed to evaluate the hydrodynamic characteristics of heat transfer within the channel. Moreover, the buoyancy effect is considered, whereas the radiation effect is neglected. The problem is solved employing the Ansys-Fluent code. Results are given in terms of stream function, fluid and solid matrix temperature fields, wall temperature profiles, air velocity and temperature as well as solid profiles along the transversal section of porous medium. *Pe* varies from 1 to 1000 and four *Ra* values are considered: 10, 50, 100 and 1000. The study evaluates the effects of *Re*, the effect of the solid wall distance and of wall heat flux on thermal and fluid dynamic behaviors. Further, Nusselt numbers and pressure drop are estimated.

2. Geometrical Description and Mathematical Formulation

A sketch of the investigated system is reported in Fig. 1.

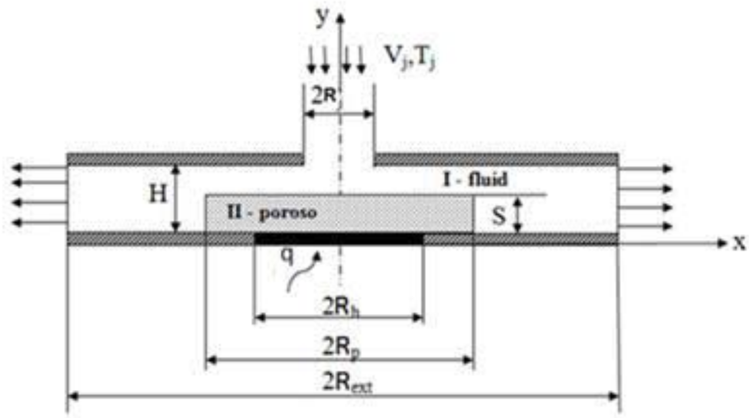

Figure 1. Geometrical and physical model with coordinate system.

The wall facing the air round jet is partially heated at uniform heat flux and the upper wall is considered adiabatic. The round jet section is equal to $2R_j$ and the channel height is H. The heat source radius is equal to R_h and the length of the lower plate is $2R_{ext}$. The unheated zone of the lower wall is assumed adiabatic.

V_j and T_j are, respectively, the velocity and the temperature of the inlet round jet. The impinging jet enters in the channel, which is partially filled by a porous medium with a thickness equal to S. In the outlet section, the flow is assumed hydro-dynamically and thermally fully developed. Air is the working fluid (Pr=0.71). Past works demonstrate that spatial variation of porosity near solid walls causes possible channeling effect in forced and in mixed convection. Actually, wall channeling increases viscous and inertial effects and the heat transfer rate, but it is particularly important for packed-sphere beds with high particle diameters. Assuming constant values of porosity and permeability, even close to a solid boundary, seems valid for metal foams and fibrous media, thanks to their relatively homogeneous structures [27-29]. The governing equations, in cylindrical coordinates, are [30]:

Continuity equation:

$$\frac{\partial u}{\partial x}+\frac{1}{r}\frac{\partial v}{\partial r}=0 \tag{1}$$

x-momentum equation:

$$\rho_f\left(\frac{1}{\varphi}\frac{\partial u}{\partial t}+\frac{u}{\varphi^2}\frac{\partial u}{\partial x}+\frac{v}{\varphi^2}\frac{\partial u}{\partial r}\right)=-\frac{\partial p}{\partial x}+\frac{\mu_f}{\varphi}\left[\frac{\partial^2 u}{\partial x^2}+\frac{1}{r}\frac{\partial}{\partial r}\left(\frac{r\partial u}{\partial r}\right)\right]-\frac{\mu u}{K}-\frac{C_F}{K^{1/2}}\rho_f\sqrt{u^2+v^2}\,u$$
$$+\rho_f g\beta_f\left(T_f-T_\infty\right) \tag{2}$$

r-momentum equation:

$$\rho_f\left(\frac{1}{\varphi}\frac{\partial v}{\partial t}+\frac{u}{\varphi^2}\frac{\partial v}{\partial x}+\frac{v}{\varphi^2}\frac{\partial v}{\partial r}\right)=-\frac{\partial p}{\partial x}+\frac{\mu_f}{\varphi}\left[\frac{\partial^2 v}{\partial x^2}+\frac{1}{r}\frac{\partial}{\partial r}\left(\frac{r\partial v}{\partial r}\right)-\frac{v}{r^2}\right]-\frac{\mu v}{K}-\frac{C_F}{K^{1/2}}\rho_f\sqrt{u^2+v^2}\,u \tag{3}$$

- Fluid phase:

Energy equation:

$$\varphi\rho_f c_{p,f}\frac{\partial T_f}{\partial t}+\rho_f c_{p,f}\left(u\frac{\partial T_f}{\partial x}+v\frac{\partial T_f}{\partial r}\right)=\varphi k_f\left[\frac{\partial^2 T_f}{\partial x^2}+\frac{1}{r}\frac{\partial}{\partial r}\left(\frac{r\partial T_f}{\partial r}\right)\right]+h_{sf}a_{sf}\left(T_s-T_f\right) \tag{4}$$

- Solid phase:

Energy equation:

$$\left(1-\varphi\right)\rho_s c\frac{\partial T_f}{\partial t}=\left(1-\varphi\right)k_f\left[\frac{\partial^2 T_s}{\partial x^2}+\frac{1}{r}\frac{\partial}{\partial r}\left(\frac{r\partial T_s}{\partial r}\right)\right]-h_{sf}a_{sf}\left(T_s-T_f\right) \tag{5}$$

where u and v are velocity components in cylindrical coordinates (x, r).

The boundary conditions are:

- Inlet section: V_j and T_j are velocity and temperature values respectively for the round jet.

- Outlet section: $\phi=u=v=T$; $\partial\varphi/\partial n=0$ (6)

- Unheated adiabatic wall: $u=v=0$; $\partial T/\partial n = 0$ (7)

The dimensionless variables are defined as:

$$\theta = \frac{T - T_\infty}{\frac{q_w H}{k_f}} \qquad E_c = \frac{p_r}{\rho_f V_r^2} \rightarrow E_c = 1 \rightarrow p_r = \rho_f V$$

$$Re = \frac{\rho_f V_r L_r}{\mu}; \quad Da = \frac{K}{L_r^2}; \quad Gr = \frac{g\beta \Delta T_r L_r^3}{v_f^2 \alpha_f}; \quad Ri = \frac{Gr}{\mathrm{Re}^2}; \quad Pe = PrRe \tag{8}$$

The average Nusselt number along the heated surface is defined as:

$$Nu_{avg} = \frac{hD_j}{k_f} \tag{9}$$

where D_j is the inner diameter of the round jet and h is the heat transfer coefficient, calculated as:

$$h = \frac{Q_{net}}{A_b (T_s - T_e)} \tag{10}$$

where Q_{net} is the net heat input, A_b is the substrate area, T_s is the average temperature of the substrate and T_e is the jet exit temperature.

3. Results and discussion

Wall temperatures for solid and fluid phases are equal, as assumed in Eq. (7). The porous medium is saturated by air (Pr = 0.71, k_f= 0.025 W/m K). Simulations are performed for assigned dimensionless lengths of the channel and the heated surface lengths. They are R/H = 5 and R_h/H =1 respectively. Da is equal to 10^{-3} and κ is equal to 10^{-4}. The dimensionless half-width of the round jet varies in the range $0.1 \leq R/H \leq 1$. Results are discussed for $1 \leq Pe \leq 1000$ and for Ra equal to 10, 50, 100, 1000. Dimensionless parameters are calculated as:

$$S = \frac{s}{H} \qquad R_p = \frac{r_p}{H} \qquad R_h = \frac{r_h}{H} \qquad R_j = \frac{r_j}{H} \qquad R_{ext} = \frac{r_{ext}}{H} \tag{11}$$

In the following, several configurations are analyzed, considering different geometrical and thermal parameters.

3.1 Configuration 1: S equal to 0.2, R_p equal to 5.

In Figure 2(a), Nu_{avg} varies in function Pe, considering four values of Ra. When Pe and Ra arise, Nu_{avg} grows. When Pe>100, curves have the same trend: values are equal changing Ra. Curves demonstrate that when *Ra*>100, forced convection is predominant; instead, when *Ra*<100, buoyancy forces are predominant. Observing temperature trend along *x*-direction in Figure 2(b), it is notable that near the spot, values are constant thanks to the high thermal conductivity of the porous medium.

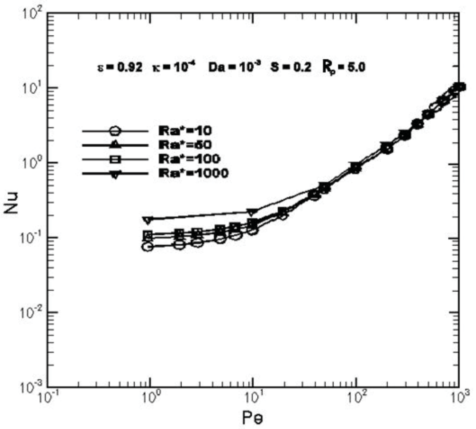

(a) Average Nusselt number as a function of Peclet number for different Rayleigh numbers

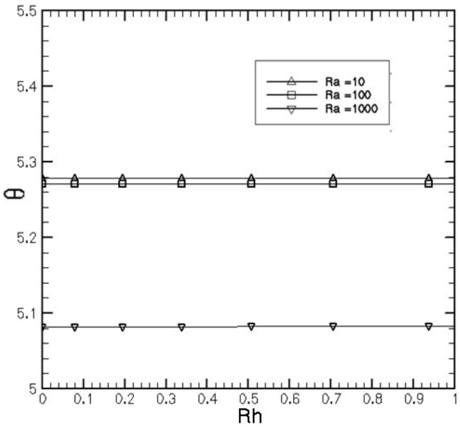

(b) Wall temperature profile as a function of R_h for different Rayleigh numbers.

Figure 2. Configuration 1: Thermal characteristics.

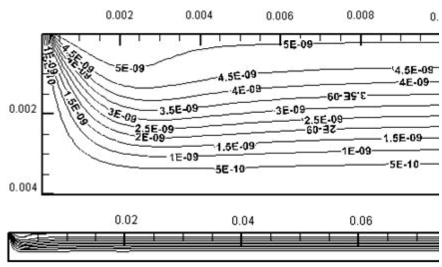

(a) *Ra* = 10.

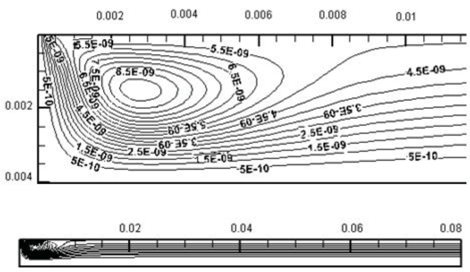

(b) *Ra* = 100

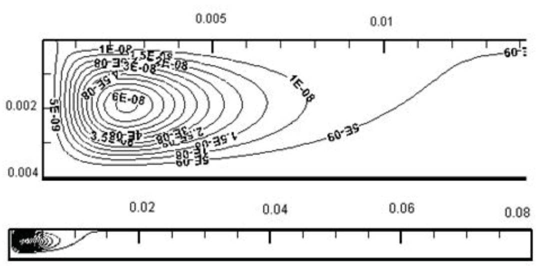

(c) *Ra* = 1000

Figure 3. Streamlines and isothermal patterns in proximity of the heated spot.

Figures 3(a), 3(b) and 3(c) show streamlines for the fixed value Pe =10, and for three different values of Ra. Greater is Ra, more variable is the flow, above all in proximity of the porous medium and greater is the swirling zone, due to buoyancy forces.

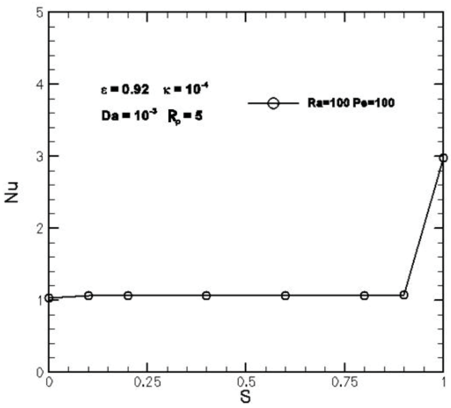

(a) Average Nusselt number as a function of S for assigned Rayleigh and Peclet numbers.

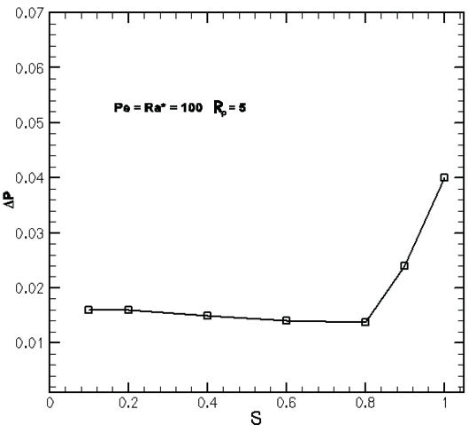

(b) Pressure drop profile as a function of S.

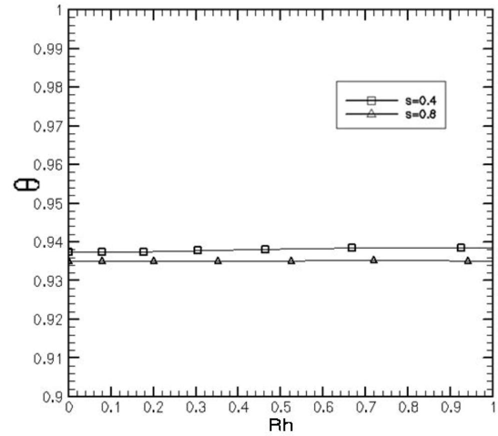

(c) Wall temperature profile as a function of R_h for different Rayleigh numbers.

Figure 4. Configuration 2: Thermal characteristics.

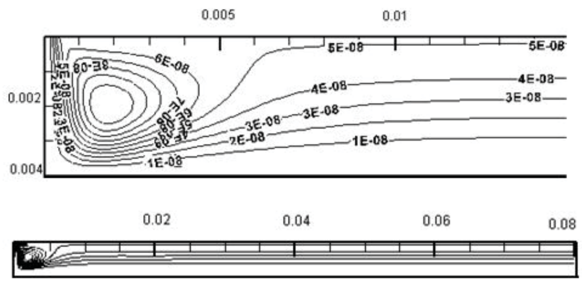

(a) S = 0.4.

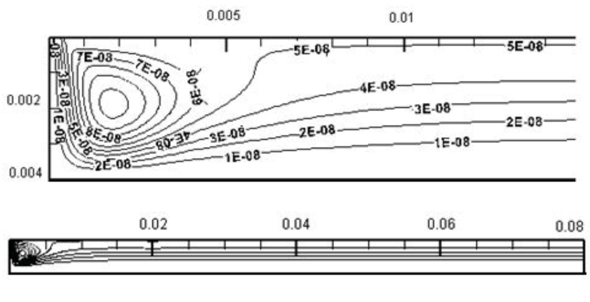

(b) S = 0.8.

Figure 5. Streamlines and isothermal patterns in proximity of the heated spot for (a) S=0.4 and (b) S=0.8.

3.2 Configuration 2: S variable, R_p equal to 5.

To optimize heat transfer, it is essential to know the *Nu* trend as a function of porous medium thickness. In Figure 4(a), *Ra* and *Pe* are constant and equal to 10; *S* is variable from 0.1(clean channel) to 1.0 (channel totally filled by porous medium). Nu_{avg} is almost constant when *S* varies from 0.1 to 0.9 and it is maximum when *S* = 1.0. The porous medium grants a higher convective heat transfer coefficient for any *S* value and this is confirmed by *ΔP*, as a function of *S*. In Figure 4(b), *ΔP* raises with *S* when *S*>0.8. These results indicate that the heat loss is the least when *S* varies from 0.4 to 0.8. Figure 4(c) shows an almost constant temperature when *S* varies from 0.4 to 0.8.

Figures 5(a) and 5(b) show streamlines and the vortex is the same for different *S* values.

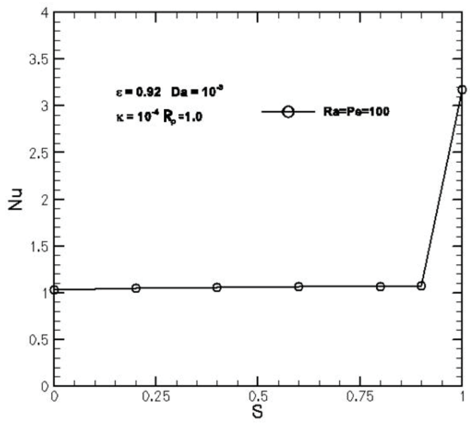

(a) Average Nusselt number as a function of *S* for assigned Rayleigh and Peclet numbers

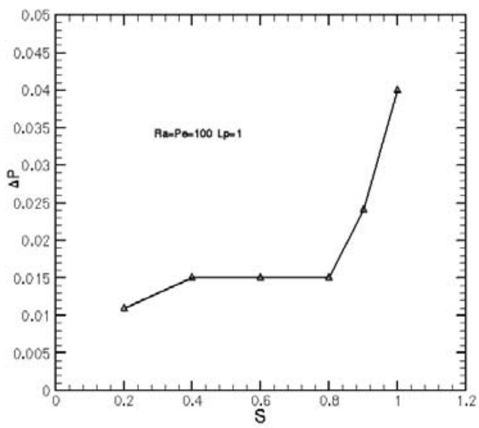

(b) Pressure drop profile as a function of *S*.

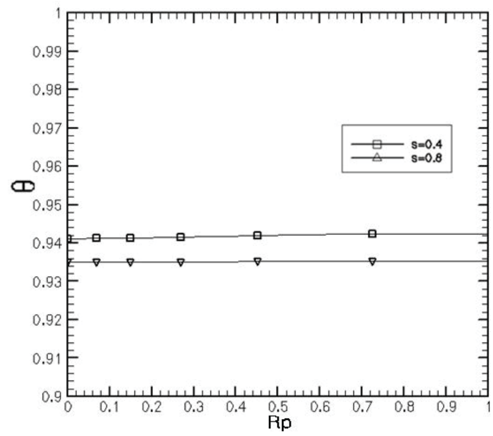

(c) Wall temperature profile as a function of R_p for different Rayleigh numbers.

Figure 6. Configuration 3: Thermal characteristics.

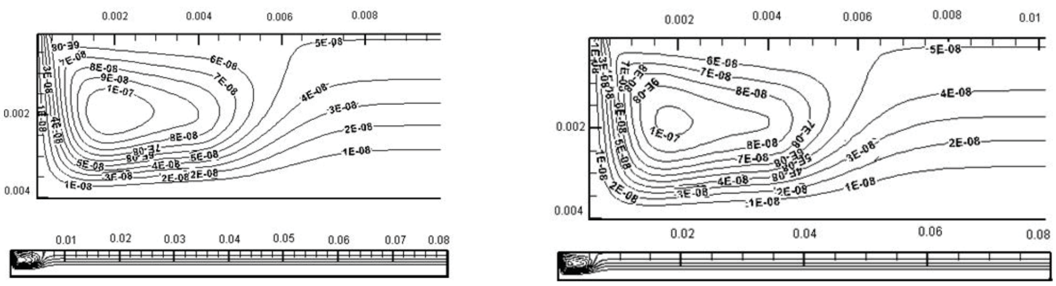

(a) $S = 0.4$. (b) $S = 0.8$

Figure 7. Streamlines and isothermal patterns in proximity of the heated spot for (a) S=0.4 and (b) S=0.8

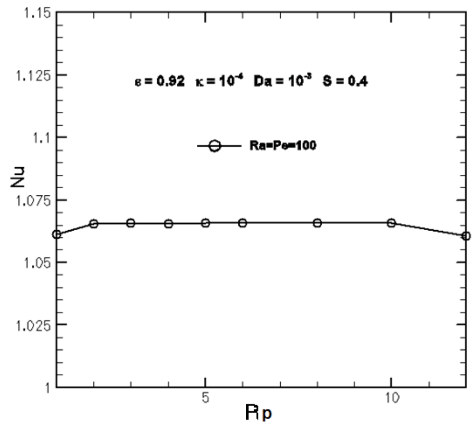

(a) Average Nusselt number as a function of R_p for assigned Rayleigh and Peclet numbers.

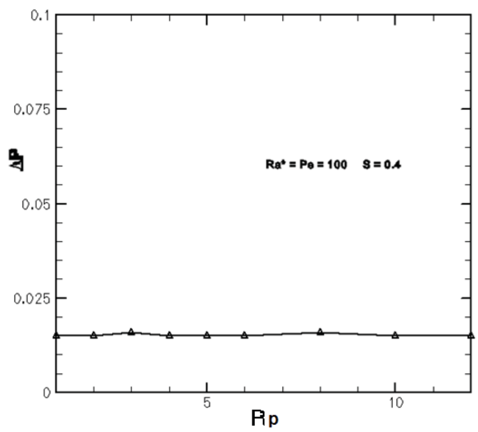

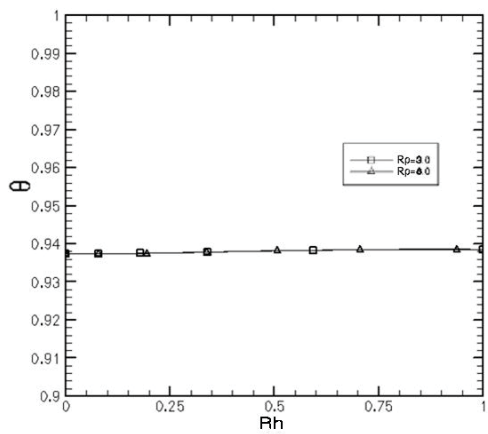

(b) Pressure drop profile as a function of R_p

(c) Wall temperature profile as a function of R_h for different R_p

Figure 8. Configuration 4: Thermal characteristics.

IOP Conf. Series: Journal of Physics: Conf. Series **796** (2017) 012012 doi:10.1088/1742-6596/796/1/012012

3.3 Configuration 3: S variable, R_p equal to 1.

In this case, the porous medium length is equal to the heated wall. *Ra* and *Pe* are equal to 100. In Figure 6(a), Nu_{avg} is almost linear, when *S* varies from 0.1 to 0.8 and it is maximum when $S = 1.0$. ΔP, in Figure 6(b), has a considerable growth when $S > 0.8$, so it is appropriate to choose a smaller *S* value. Figure 6(c) shows an almost constant temperature when *S* is equal to 0.4 and to 0.8.

Figures 7(a) and 7(b) show streamlines and the vortex is the same for different *S* values.

3.4 Configuration 4: S equal to 0.4, R_p variable.

Now, the *S* value is fixed and R_p varies from 1 to 12, considering $Ra = Pe = 100$. In Figure 8(a), Nu_{avg} stabilizes when R_p>8, so the porous medium is not necessary. When $R_p = 12$, Nu_{avg} decreases, because vortexes make worse the heat change, so the most suitable value of R_p is smaller than 10. ΔP, in Figure 8(b), does not change considerably with R_p. These results prove that, for $S = 0.4$, the most suitable value of R_p is 2. Figure 8(c) shows an almost constant temperature when R_p varies from 3 to 8.

Figures 9(a) and 9(b) show streamlines and the vortex is the same for different *S* values.

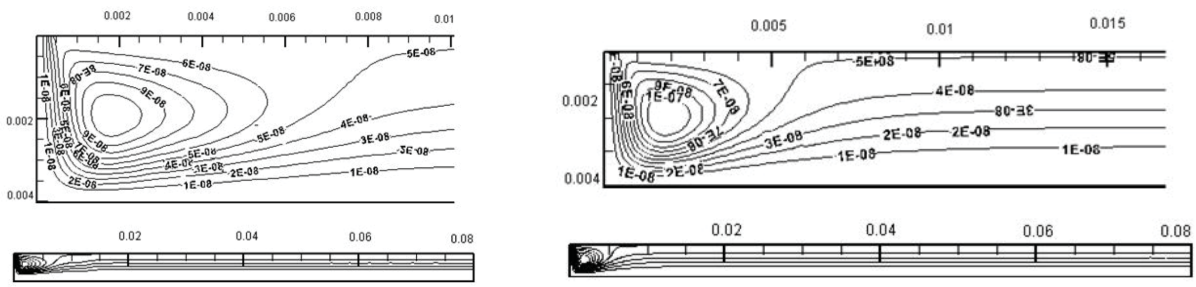

(a) $R_p = 3$. (b) $R_p = 8$.

Figure 9. Streamlines and isothermal patterns in proximity of the heated spot for (a) R_p=3 and (b) R_p=8.

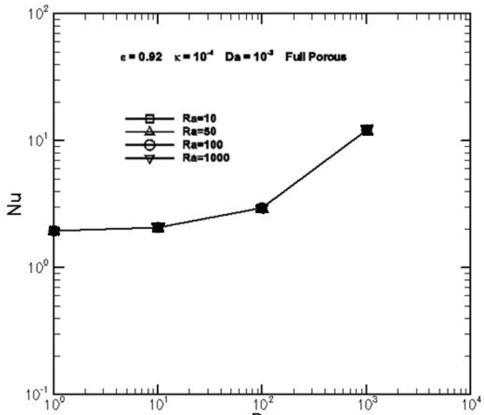

Figure 10. Average Nusselt number as a function of *Pe* for different Rayleigh numbers.

3.5 Configuration 5: S equal to 1 (channel totally filled).

In this chase, the channel is totally filled by the porous medium. Figure 10 shows that curves coincide for different values of *Ra*: Nu_{avg} is not influenced by *Ra*, because solid medium heat conductivity is greater then fluid medium ($k = 10^{-4}$), so solid temperature drops are negligible and buoyancy forces are weak. Figures 11(a) and 11(b) show that streamlines are the same for different values of *Ra*.

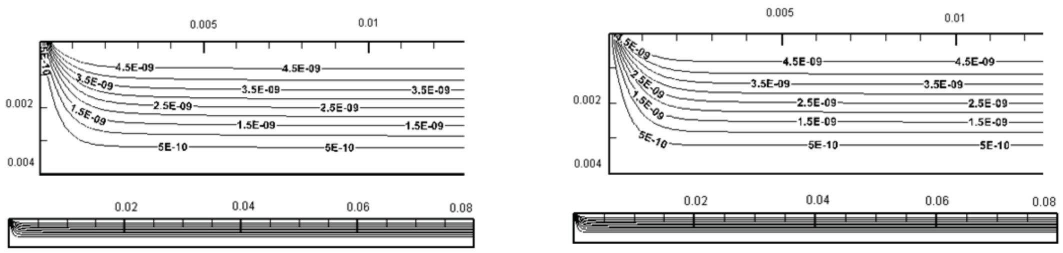

(a) Ra = 10. (b) Ra = 100.

Figure 11. Streamlines and isothermal patterns in proximity of the heated spot for (a) *Ra*=10 and (b) *Ra*=100.

Furthermore, the heat transfer coefficient ratio, h_m/h_c, is analyzed in the following, as a function of *S* and R_p, for assigned *Ra* and *Pe* ($Ra = Pe = 100$). As shown in Figure 12(a), if *S* varies from 0.2 to 0.8, h_m/h_c does not arise considerably with or without porous medium but it is noticeable when *S* is equal to the channel height. In Figure 12(b), if $R_p < 3$, h_m/h_c arise considerably with or without porous medium, so in this range heat losses are the smallest.

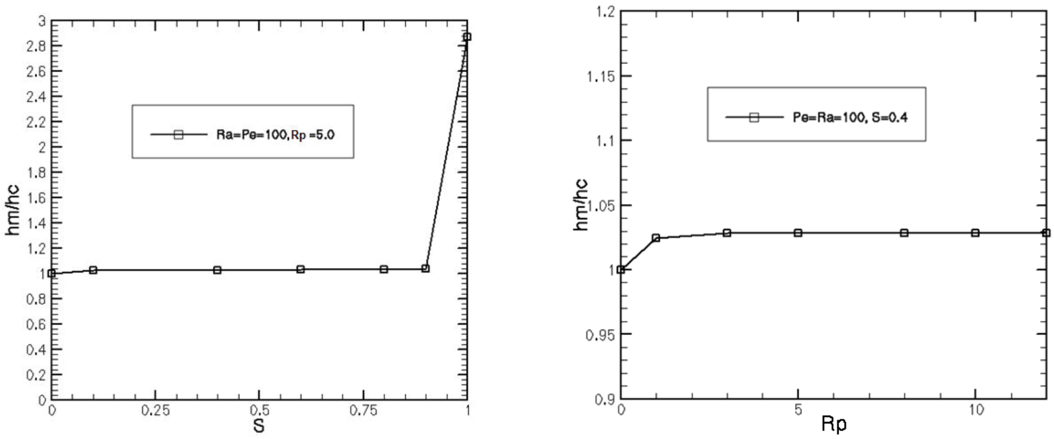

(a) In function of *S* for assigned *Ra*, *Pe*, R_p. (b) In function of R_p for assigned *Ra*, *Pe*, *S*.

Figure 12. Heat transfer coefficient ratio.

4. Conclusions

A parallel-plate channel filled partially with a high permeability porous medium and a single round jet impinging on the porous medium are numerically investigated. The opposite wall to the air round jet is partially heated at uniform heat flux. The fluid flow in the channel is assumed two dimensional and the porous medium is modeled using the Brinkman–Forchheimer-extended Darcy model. The porous medium structure is homogenous and isotropic, the thermophysical properties considered temperature independent. The analysis in the porous medium is accomplished under local thermal equilibrium conditions.

Analyzing five different configurations, studies reveal the correlation between Nusselt number and Rayleigh and Peclet numbers. For assigned S and R_p (Configuration 1), when Pe and Ra arise, Nu_{avg} grows, but if $Pe > 100$, Nu_{avg} values are equal changing Ra. Varying S (Configurations 2 and 3), results indicate that the heat loss is the least when S varies from 0.4 to 0.8 and the vortex zones are similar for each S. For assigned R_p and varying S (Configuration 4), the average Nusselt number, Nu_{avg}, stabilizes when $R_p > 8$, so the porous medium is not necessary. The study of the correlation between average Nusselt number and porous medium thickness (Configuration 5) optimizes heat transfer system. In particular, the presence of porous medium increases the heat transfer near the heated bottom wall, so when the channel is totally filled by the porous medium, Nu_{avg} is not influenced by Ra, cause solid medium heat conductivity is greater then fluid medium, solid temperature differences are negligible and buoyancy forces are weak.

5. Nomenclature

a_{sf}	specific surface area, m^2/m^3
Bi	Biot-like number
C_F	inertia coefficient
D	width of the jet, m
Da	Darcy number
g	gravitational acceleration, ms^{-2}
H	width of the channel, m
R	round slot radius, m
h_{sf}	interstitial heat transfer coeff., Wm^{-2}K^{-1}
k	thermal conductivity, Wm^{-1}K^{-1}
K	permeability, m^2
R_h	half of the heat source length, m
Ra	Rayleigh number
Nu_{avg}	average Nusselt number
Pr	Prandtl number
q	heat flux, Wm^{-2}
Pe	Peclet number
T	temperature, K
u,v	velocity components, ms^{-1}
U,V	dimensionless velocity components
x,y	Cartesian coordinates, m
X,Y	dimensionless Cartesian coordinates
ΔP	pressure drop

Greek Symbols

α	thermal diffusivity, m^{2}s^{-1}
β	volumetric expansion coefficient, K^{-1}
γ	modified conductivity ratio
ϑ	dimensionless temperature
κ	effective thermal conductivity ratio
ν	kinematic viscosity, m^{2}s^{-1}
φ	porosity
ρ	density, kg m^{-3}

Subscripts

eff	effective
f	fluid
j	jet
s	solid
w	wall
avg	average

6. References

[1] Han B and Goldstein RJ 2001 *Ann. New York Acad. Sciences* **934** 147.
[2] Wright WB 2004 *AIAA Paper* 4153.
[3] Agostini B, Fabbri M, Park JE, Wojtan L, Thome JR and Michel B 2007 *Heat Transfer Eng.* **28** 258.
[4] Ebadian MA and Lin CX 2011 *ASME J. Heat Transfer* **133** art. no. 110801.
[5] Gururatana S 2012 *Am. J. App. Sciences* **9** 436.
[6] Andrei L, Carcasci C, Da Soghe R, Facchini B, Maiuolo F, Tarchi L and Zecchi S 2013 *ASME J. Turbomach.* **135** art. no. 031020.
[7] Viskanta R 1993 *Exp Therm. Fluid Science* **6** 111.
[8] Polat S 1993 *Drying Tech* **11** 1147.

[9] Iacovides H and Launder BE 1995 *Int. J. Heat Fluid Flow* **16** 454.
[10] Baukal CE Jr. and Gebhart B 1996 *Int. J. Heat Fluid Flow* **17** 386.
[11] Fu WS and Huang HC 1997 *Int. J. Heat Mass Transfer* **40** 2261.
[12] Jeng TM and Tzeng SC 2005 *Int. J. Heat Mass Transfer* **48** 4685.
[13] Saeid NH and Mohamad AA 2006 *Int. J. Heat Mass Transfer* **49** 3906.
[14] Saeid NH 2007 *Int. J. Heat Mass Transfer* **50** 4265.
[15] Sivasamy A, Selladurai V and Kanna PR 2010 *Int. J. Heat Mass Transfer* **53** 5847.
[16] Sivasamy A, Selladurai V and Kanna PR 2010 *Int. J. Therm. Sciences* **49** 1238.
[17] Wong KC and Saeid NH 2009 *Int. Comm. Heat Mass Transfer* **36** 45.
[18] Wong KC and Saeid NH 2009 *Int. J. Therm. Sciences* **48** 96.
[19] Wong KC and Saeid NH 2009 *Int. Comm. Heat Mass Transfer* **36** 155.
[20] Sivasamy A, Kanna PR and Selladurai V 2011 *Int. J. Heat Mass Transfer* **54** 4127.
[21] Buonomo B, Manca O and Nardini S 2012 *4th Int. Conf. Porous Media and its Applications in Science and Engineering, ICPM4*, June 17-22, Potsdam, Germany.
[22] Lam PAK and Prakash KA 2015 *Energy Conv. Manag.* **89** 626.
[23] Shih WH, Chou FC and Hsieh WH 2007 *ASME J. Heat Transfer* **129** 1554.
[24] Yakkatelli R, Wu Q and Fleisher AS 2010 *Exp Thermal Fluid Science* **34** 1008.
[25] Feng SS, Kuang JJ, Wen T, Lu TJ and Ichimiy K 2014 *Int. J. Heat Mass Transfer* **77** 1063.
[26] Lee CH, Lim KB, Lee SH, Yoon YJ and Sung NW 2007 *Exp Thermal Fluid Science* **31** 559.
[27] Hunt ML and Tien CL 1988 *Int. J. Heat Mass Transfer* **31** 301.
[28] Jeng TM and Tzeng SC 2008 *Int. Comm. Heat Mass Transfer* **35** 30.
[29] Lee DY and Vafai K 1999 *Int. J. Heat Mass Transfer* **42** 423.
[30] Buonomo B, Manca O and Nardini S 2015, *Handbook of Porous Media, Third Edition, edited by Kambiz Vafai*, CRC Press 631.